scientific reports

Check for updates

OPEN

The microbial metabolite *p*-cresol compromises the vascular barrier and induces endothelial cytotoxicity and inflammation in a 3D human vessel-on-a-chip

Sakulrat Mankhong[1,4], Thittaya Den-Udom[1,2,4], Tanotnon Tanawattanasuntorn[1], Thunwarat Suriyun[1], Kenjiro Muta[1], Chagriya Kitiyakara[3] & Pimonrat Ketsawatsomkron[1]✉

Increased protein-bound uremic toxins (PBUTs) in patients with chronic kidney disease (CKD) are associated with cardiovascular diseases (CVDs); however, whether retention of PBUTs causes CVD remains unclear. Previous studies assessing the impacts of PBUTs on the vasculature have relied on 2D cell cultures lacking in vivo microenvironments. Here, we investigated the impact of various PBUTs (p-cresol (PC), indoxyl sulfate (IS), and p-cresyl sulfate (PCS)) on microvascular function using an organ-on-a-chip (OOC). Human umbilical vein endothelial cells were used to develop 3D vessels. Chronic exposure to PC resulted in significant vascular leakage compared with controls, whereas IS or PCS treatment did not alter the permeability of 3D vessels. Increased permeability induced by PC was correlated with derangement of cell adherens junction complex, vascular endothelial (VE)-cadherin and filamentous (F)-actin. Additionally, PC decreased endothelial viability in a concentration-dependent manner with a lower IC_{50} in 3D vessels than in 2D cultures. IS slightly decreased cell viability, while PCS did not affect viability. PC induced inflammatory responses by increasing monocyte adhesion to endothelial surfaces of 3D vessels and IL-6 production. In conclusion, this study leveraged an OOC to determine the diverse effects of PBUTs, demonstrating that PC accumulation is detrimental to ECs during kidney insufficiency.

Keywords Uremic toxins, Endothelial cells, Vasculature, Organ-on-a-chip

The vascular endothelium plays an essential role in maintaining homeostasis in the cardiovascular system by regulating blood flow, vascular permeability, and inflammatory responses[1]. Endothelial dysfunction underlies the pathogenesis of cardiovascular diseases (CVDs) and presents at an early stage in chronic kidney disease (CKD)[2,3]. In fact, cardiovascular mortality is increased 500–1000-fold in patients with end-stage kidney disease compared with the general population[4], suggesting that kidney-related mechanisms possibly mediate CVD. Particularly, an accumulation of protein-bound uremic toxins (PBUTs) are associated with cardiovascular morbidity and mortality in patients with CKD[5,6]. Elevated PBUTs including p-cresol (PC), p-cresyl sulfate (PCS), and indoxyl sulfate (IS) have been repeatedly reported in patients with CKD[7,8]. However, whether these PBUTs contribute to the rapid progression of CVD in patients with renal diseases is unknown.

PBUTs, a class of uremic toxins (UTs), are amino acid metabolites generated by intestinal bacteria[9]. Specifically, PC is a product of tyrosine metabolism in the gut[9], which is primarily converted to PCS through sulfonation in the liver before entering systemic circulation[9,10]. In addition, tryptophan metabolism by gut microbiota and liver enzymes generates circulating IS[9,11]. In healthy subjects, PBUTs are effectively removed by the kidneys[12]; however, their clearance is compromised in patients with CKD and they are difficult to remove by hemodialysis because of their high affinity towards serum proteins (such as albumin), resulting in their retention[12]. Various

[1]Chakri Naruebodindra Medical Institute, Faculty of Medicine Ramathibodi Hospital, Mahidol University, 111 Moo 14, Bang Pla, Bang Phli, Samut Prakan 10540, Thailand. [2]Program in Translational Medicine, Faculty of Medicine Ramathibodi Hospital, Mahidol University, Bangkok, Thailand. [3]Department of Medicine, Faculty of Medicine Ramathibodi Hospital, Mahidol University, Bangkok, Thailand. [4]These authors contributed equally: Sakulrat Mankhong and Thittaya Den-Udom. ✉email: pimonrat.ket@mahidol.edu

PBUTs have been shown to exert direct detrimental effects on different cell types in cardiovascular system, thus contributing to CVD pathogenesis. Although the clinical correlation between increased PBUTs and CVD risk has long been discussed[13], the causality of UTs in CKD has yet to be proven[14] and their mechanistic roles remain to be explored. It remains inconclusive whether removal of UTs (such as by AST-120) can delay CKD disease progression in humans[15,16]. In fact, more recent evidence has indicated that not all UT metabolites are toxic and that they have diverse biological activities[17]. Because of this, the roles of PBUTs in CVD need to be studied and redefined.

Although the cardiovascular impact of PBUTs has been actively investigated, prior findings have relied mostly on studies using conventional 2D cell cultures. The lack of a physiologically relevant microenvironment in 2D cultures poses significant limitations[18–20]. Indeed, hemodynamic shear stress generated by blood flow is critical for endothelial cell function and vascular permeability[21]. Moreover, interactions between EC and ECM regulate EC apoptosis, proliferation, cytoskeletal changes, and cell shape alterations[22]. Recently, advances in organ-on-a-chip (OOC) technology have provided a powerful tool for interrogating EC functions in a 3D microenvironment. OOCs allow the assembly of human ECs into 3D geometry under exposure to luminal shear flow and complex cellular interactions with ECM. Consequently, vessel OOCs display gene expression and drug responses closer to human conditions than 2D cultures[23–25]. In the present study, we tested the hypothesis that there are differential effects of PBUTs (PC, IS, and PCS) on vascular function using a perfused 3D human vessel-on-a-chip. Our findings are in line with those of previous reports describing the detrimental effects of specific UTs on vasculatures and unravel the differential impacts of PBUTs on the endothelium.

Results

Characterization of 3D human vessel-on-a-chip

To develop human 3D vessels, we used two-lane Organoplates (Mimetas, the Netherlands) (Supplementary Fig. 1A and B). Human umbilical vein endothelial cells (HUVECs) were cultured against the collagen (Fig. 1A) and the 3D reconstruction of confocal images showed self-assembled EC monolayers with luminal and basolateral surfaces (Fig. 1B and Supplementary Video 1). The 3D vessels abundantly expressed an endothelial cell marker (CD31; Supplementary Fig. 1C) and maintained their viability for at least 14 days (Fig. 1C) with an incremental increase in WST-8 activity over time. We observed cell migration to the ECM channel after 7 days of cell seeding (*data not shown*); because of this, subsequent experiments were performed before day 7. Staining of 3D vessels with calcein-AM (LIVE) on day 5 confirmed abundant live ECs, while dead cells were barely detectable with ethidium homodimer-1 (DEAD) (Fig. 1D).

Following this, we tested if the 3D vessels developed barriers restrictive to macromolecules. Time-lapse studies were conducted to investigate the vascular leakage from the luminal to the basolateral surface of 70 kDa FITC dextran, a molecule that has a similar molecular weight to albumin. 3D vessels exhibited markedly less FITC dextran accumulation in ECM than cell-free groups (Fig. 1E), indicating a macromolecule-restricted barrier in 3D vessels. The average of the apparent permeability coefficient (Papp) was markedly lower in 3D vessels compared with cell-free controls (Papp: 3D vessel = 1.7×10^{-6} cm/s vs. cell-free = 9×10^{-6} cm/s, $p < 0.05$) (Fig. 1F). We also determined the effects of TNFα, a cytokine known to induce vascular leakage[26], on the integrity of the 3D vascular barrier. As expected, TNFα increased the permeability of 3D vessels compared with vehicle treatment (Supplementary Fig. 2). Taken together, we concluded that the 3D vessels established in the Organoplate maintained stable tubular structures and cell viability for at least 14 days, and ECs formed an impermeable barrier to a physiologically relevant-sized macromolecule.

Distinct impact of UTs on 3D vessel permeability

In this study, we investigated the impact of PBUTs on 3D vessel barrier. On the third day post-cell seeding, 3D vessels were treated with PC, IS, or PCS for 72 h before vascular permeability to sized molecules was examined. Stimulation of 3D vessels with PC for 72 h significantly increased vascular permeability to 70 kDa dextran in a concentration-dependent manner compared with vehicle-treated controls (Fig. 2A, B, Supplementary Video 2A) (Papp: 200 μM PC = 5.2×10^{-6} cm/s, 400 μM PC = 7.4×10^{-6} cm/s vs. vehicle = 1.4×10^{-6} cm/s, $p < 0.05$). Similarly, PC significantly compromised the EC barrier to 10 kDa dextran (Fig. 2C, D, Supplementary Video 2B) (Papp: 200 μM PC = 11.7×10^{-6} cm/s, 400 μM PC = 15.6×10^{-6} cm/s vs. vehicle = 4.8×10^{-6} cm/s, $p < 0.05$). The morphology of ECs following PC exposure for 72 h is shown in Supplementary Fig. 3. The 24-h treatment of 3D vessels with PC tended to increase vascular leakage (Papp: 200 μM PC = 2.3×10^{-6} cm/s, 400 μM PC = 2.8×10^{-6} cm/s vs. vehicle 1.5×10^{-6} cm/s, $p > 0.05$) (Supplementary Fig. 4), but the effect was more robust with prolonged stimulation (72 h). Unlike PC, prolonged stimulation of 3D vessels with either IS or PCS (200 or 400 μM) did not alter the EC barrier integrity to 70 kDa and 10 kDa FITC dextran when compared with the vehicle-treated controls (Fig. 3A, B for IS; Fig. 3C, D for PCS). From these studies, we conclude that the examined PBUTs differentially affected the endothelial barrier of 3D vessels.

Effects of PC on vascular endothelial (VE)-cadherin and filamentous (F)-actin stress fibers

VE-cadherin is the major determinant in maintaining vascular integrity[27]. The interaction between VE-cadherin and the actin cytoskeleton plays a crucial role in endothelial barrier maintenance[28–30]. Derangement of VE-cadherin at cell–cell junctions and the formation of actin stress fibers lead to vascular leakage[31,32]. We next evaluated the effects of PC on morphology and localization of VE-cadherin and cellular filamentous actin (F-actin). As expected, interaction of VE-cadherin (green) and stress fibers (red) was visualized at cell–cell contacts in 3D vessels treated with vehicle (Fig. 4). PC stimulation for 72 h did not decrease VE-cadherin expression but increased F-actin stress fiber formation (Fig. 4). There was an increase in stress fiber with elevated PC concentration (Supplementary Fig. 5). Importantly, PC led to the disassembly of VE-cadherin and F-actin as indicated by Pearson's correlation coefficient (Pearson's R, which represents their co-localization[33]), which was lower in PC-treated

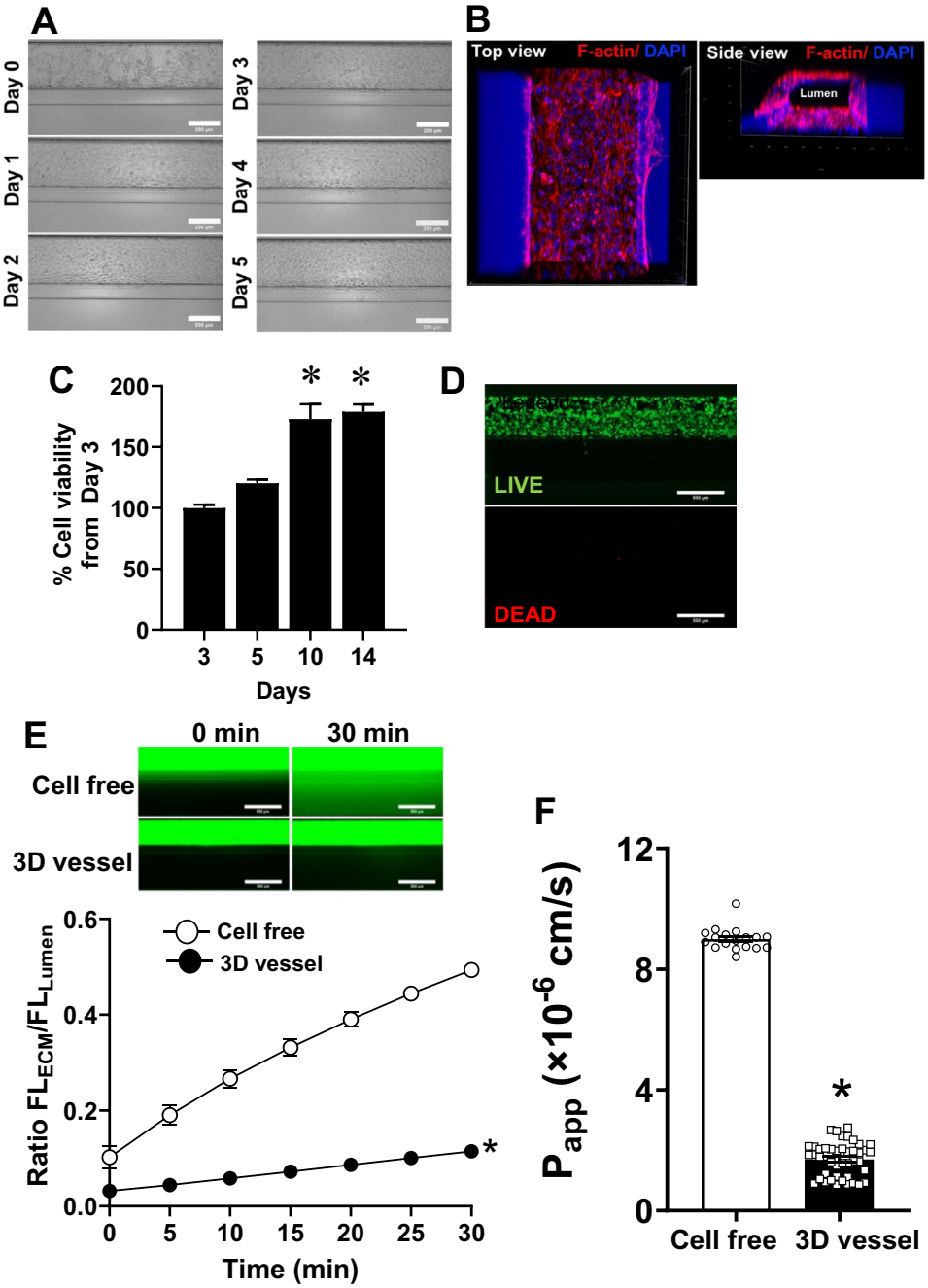

Figure 1. Characterization of human EC vessel-on-a-chip. (**A**) Typical characteristics of EC human vessels following cell seeding; 5X Bright-field images, scale bar: 200 µm (**B**) Confocal images (magnification: 10X) showing the 3D structure of human vessels with luminal and basolateral surfaces (red = F-actin; blue = DAPI). (**C**) Quantitative measurement of cell viability in EC vessels on days 3, 5, 10, and 14 after HUVECs seeding; n = 12. (**D**) Live/dead staining of EC vessels on day 5; green represents live signals, while red indicates dead cells (n = 5, magnification: 5X, scale bar: 500 µm). (**E**) Permeability assay with 70 kDa FITC dextran in EC vessels compared with cell-free controls. (Top) Representative time-lapse images to monitor fluorescently labeled dextran leakage to the adjacent collagen channel over 30 min. (Bottom) Quantitative fluorescence intensity ratio of the ECM to the lumen. Two-way repeated measures ANOVA followed by post hoc testing were used; $^{*}p < 0.05$ versus cell-free (n = 8–22). (**F**) Summary of apparent permeability (Papp) of 70 kDa dextran; unpaired t-test, $^{*}p < 0.05$ versus cell-free (n = 18 for cell-free and n = 44 for EC vessels).

3D vessels than in vehicle-treated controls (Fig. 4A). Taken together, the observed PC-induced derangement of VE-cadherin and the cellular cytoskeleton was consistent with the hyperpermeability of 3D vessels.

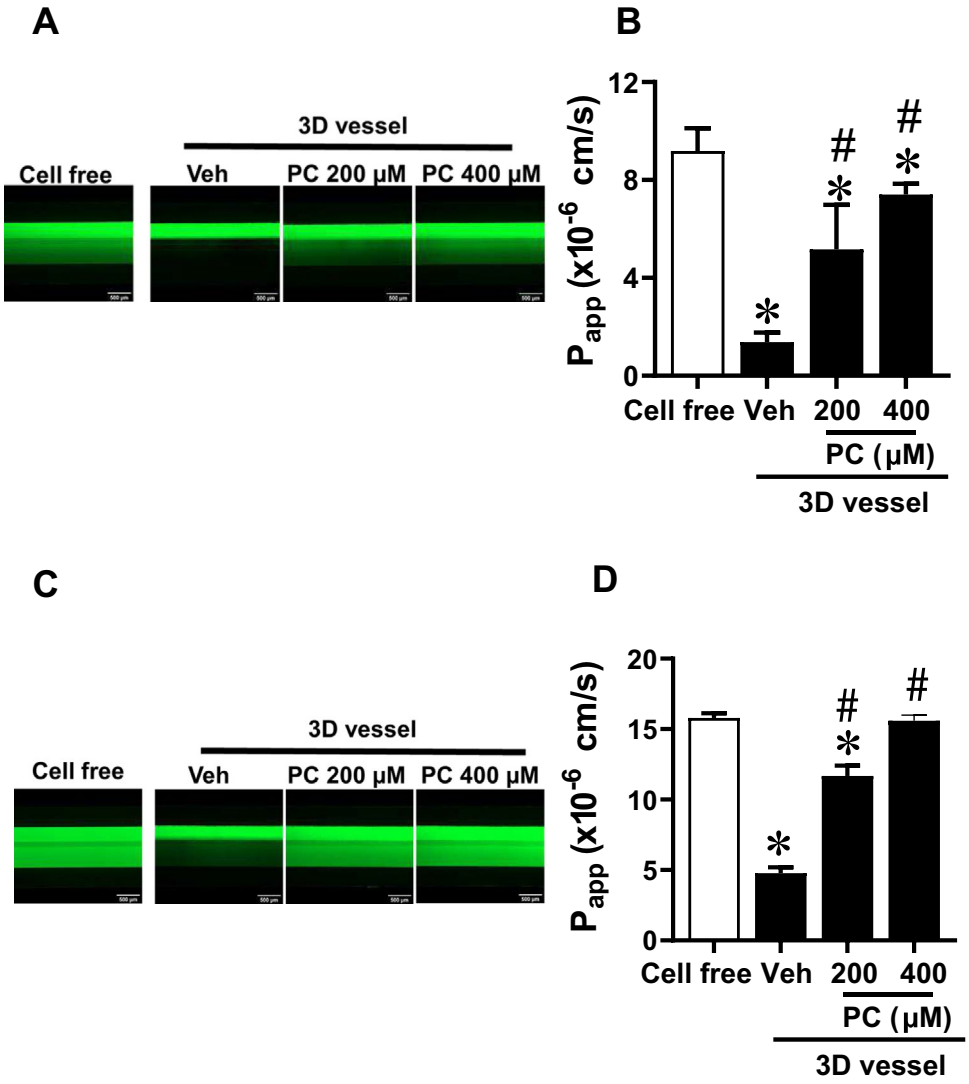

Figure 2. EC vessel permeability after 72 h of p-cresol (PC) treatment. Vessels were stimulated with either vehicle (Veh), 200 μM, or 400 μM of PC for 72 h before vascular permeability was determined. (**A**) Representative time-lapse images at 30 min of 70 kDa FITC-dextran and (**B**) apparent permeability (Papp) of 70 kDa dextran. (**C**) Representative time-lapse images at 30 min of 10 kDa FITC-dextran and (**D**) apparent permeability (Papp) of 10 kDa dextran. Magnification: 4X; scale bar: 500 μm. Data are mean ± SEM, n = 9–20. One-way ANOVA multiple comparisons were used for Papp; $^{*}p < 0.05$ versus cell-free, $^{\#}p < 0.05$ versus Veh.

Increased cytotoxicity caused by PC

Next, we investigated the potential cytotoxicity impact of PBUTs in 3D vessels. We first validated the reliability of the WST-8 cell viability assay in 3D vessels using cisplatin, an anti-tumor drug known to induce EC cytotoxicity[34]. Expectedly, 3D ECs treated with 100 μM cisplatin had decreased cell viability compared with vehicle-treated controls (Supplementary Fig. 6). The WST-8 assay in 3D vessels achieved a robust Z' value (0.42), which is considered good for compound screening[35]. We then evaluated the cell viability of 3D vessels after stimulation with PC, IS, and PCS at different concentrations for 72 h. PC treatment induced a significant cytotoxic effect in a concentration-dependent manner (Fig. 5A). Additionally, we compared the IC_{50} of PC-induced cytotoxicity between 3D vessels and 2D HUVEC cultures. PC treatment yielded $IC_{50} = 805.3 \pm 144.4$ μM in the 2D cultures, while it was 340.4 ± 25 μM in 3D vessels ($p < 0.05$, t-test) (Fig. 5B). This demonstrated that ECs cultured in 3D vessels were more susceptible to PC-induced cytotoxicity than 2D HUVEC cultures. In contrast to PC, IS caused a modest decrease in EC viability only at high concentrations (800 and 1000 μM), while PCS did not cause cytotoxicity in 3D vessels (Fig. 5C, D).

Increased endothelial inflammation caused by PC

To assess whether PC stimulation caused inflammatory responses in 3D vessels, monocyte adhesion to endothelium and production of IL-6 (a pro-inflammatory cytokine) were evaluated. We first validated the monocyte

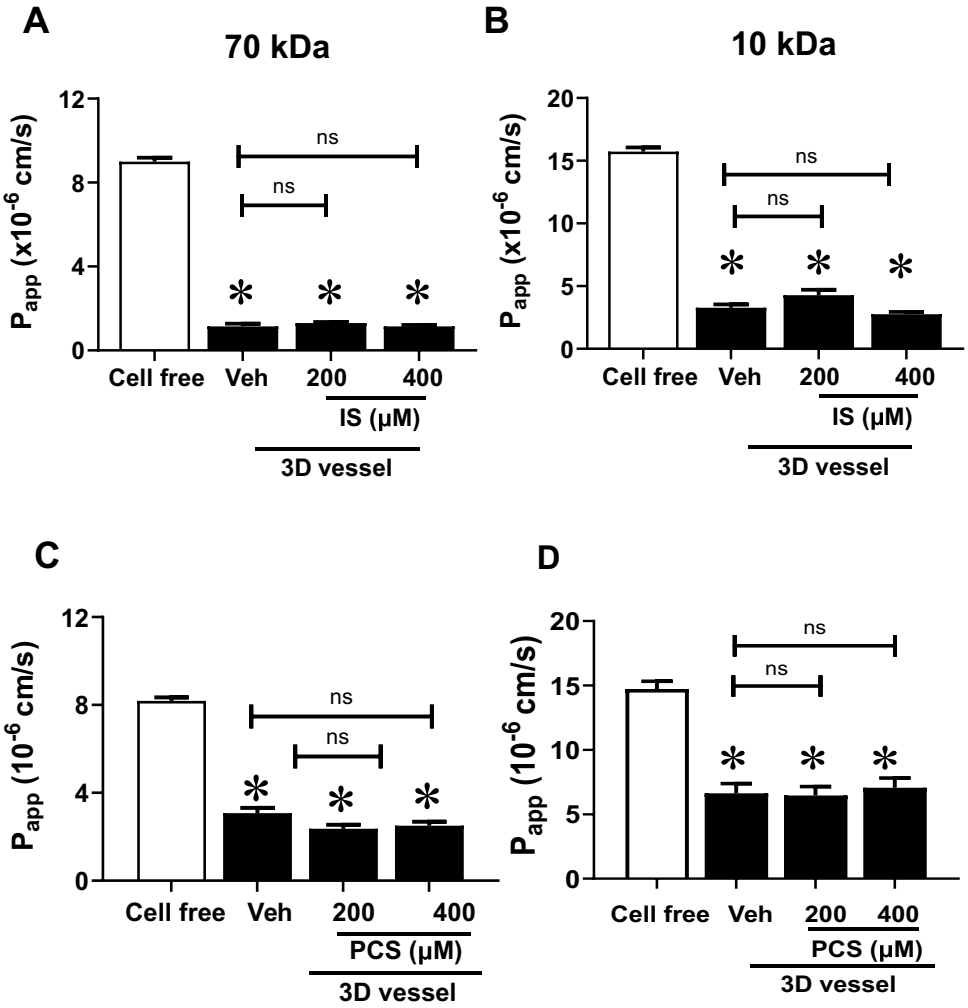

Figure 3. 3D vessel permeability after 72 h of indoxyl sulfate (IS) and p-cresyl sulfate (PCS) treatment. Vessels were exposed to either vehicle (Veh) or different concentrations of IS (200 and 400 μM) for 72 h before vascular permeability was determined. (**A**) and (**B**) Apparent permeability (Papp) of 70 kDa and 10 kDa dextran, respectively. (**C**) and (**D**) Papp of 70 kDa and 10 kDa dextran, respectively, of 3D vessels-treated with either vehicle (Veh) or different concentrations of PCS (200 and 400 μM) for 72 h before vascular permeability was determined. Data are mean ± SEM, n = 5–19. One-way ANOVA multiple comparisons were used for Papp; $^{*}p < 0.05$ versus cell-free, ns = not significant.

adhesion and IL-6 production assays in 3D vessels using TNFα. There were increases in monocyte adherence and IL-6 release relative to vehicle treatment after TNFα stimulation (Fig. 6A, B). PC treatment at 400 μM but not at 200 μM led to elevated monocyte adhesion to the luminal surface of 3D vessels compared with vehicle-treated controls (Fig. 6C). Additionally, there was a significant increase in IL-6 following PC treatment (Fig. 6D). Taken together, these results show that exposure of perfused 3D vessels to PC led to endothelial inflammatory responses.

Discussion

Endothelial dysfunction manifests at an early stage in patients with CKD[36] and contributes to the development of CVDs[3,37,38]. Despite strict control of typical CVD risk factors such as hypertension, dyslipidemia, and hyperglycemia with common treatments, residual cardiovascular risks remain high in patients with CKD[39]. Other risk factors specific to renal insufficiency contribute to CVD pathogenesis in this population[40]. Among different possible mechanisms, retention of PBUTs is associated with cardiovascular morbidity and mortality in patients with CKD[5,6]. Here, we examined the effects of three PBUTs that are commonly elevated in patients with CKD on endothelial function using a perfused human vessel-on-a-chip. We observed that prolonged exposure of 3D human vessels to PC led to a compromised vascular barrier that was correlated with derangement of VE-cadherin and F-actin localization, reduced endothelial viability, increased monocyte adhesion to endothelial surface, and elevated IL-6 production. Notably, ECs from 3D vessels were more susceptible to PC-induced endothelial cytotoxicity than those from 2D HUVEC cultures. However, we reported that only high concentrations (800 and 1000 μM) of IS decreased endothelial viability in 3D vessels, while PCS did not have any impact. These

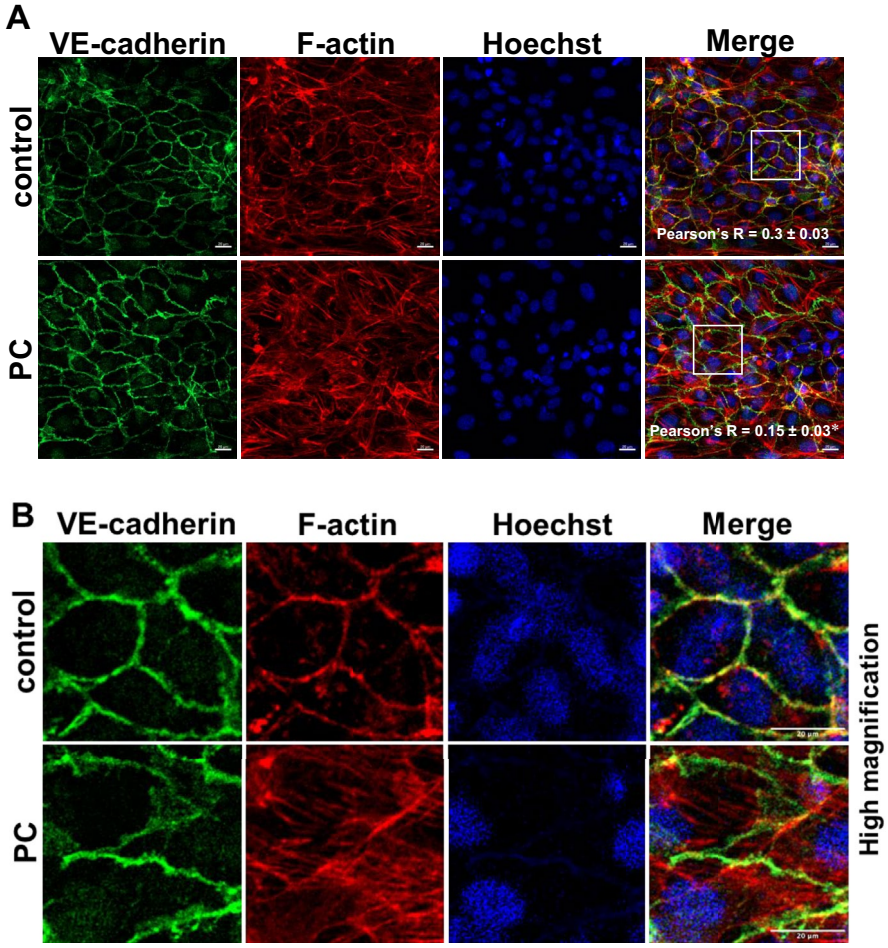

Figure 4. The impact of p-cresol (PC) on VE-cadherin and F-actin stress fibers. (**A**) Immunostaining of 3D vessels for VE-cadherin (green), F-actin (red), and nuclei (blue) after treatment with PC at 200 µM for 72 h. Magnification: 20x; scale bar: 20 µm. Pearson's R correlation coefficient was significantly lower in PC-treated cells when compared with vehicle controls. Images shown and used for all analysis were taken using maximum projection. Data are mean ± SEM, n = 3, $*p < 0.05$, t-test. White boxes indicate high magnification images shown in (**B**). Cropped images of 420 × 420 pixel ROIs from Fig. 4A, scale bar: 20 µm.

results provide additional evidence to support the notion that the accumulation of PC in patients with CKD is detrimental to the vasculature, possibly contributing to CVD pathogenesis.

Even though previous studies have focused on the negative impact of IS and PCS in CVD, as these PBUTs are elevated in the plasma of patients with CKD[41], the significance of PC should not be overlooked. Previous reports have demonstrated that PC is relatively more toxic than its metabolites; for example, exposure to PC inhibited endothelial progenitor cell proliferation, arrested the cell cycle, and limited blood vessel formation, while PCS did not[42]. Similarly, PC was more potent than PCS when causing increased LDL uptake in macrophages, which was associated with more extensive lipid depositions in the aorta[43]. Together with our findings, these results suggest that PCS is the product of detoxification of elevated PC[44]. It is important to note that in vitro testing of PBUTs, including our current studies, has mostly been conducted under normal conditions without other pathological perturbations. Such risk factors, including hypertension and diabetes, are often prevalent in patients with CKD[45]. It is well recognized that increased systemic blood pressure and hyperglycemia are closely associated with endothelial dysfunction, known as a hallmark of CVD, which is attributed to reduced nitric oxide (NO) bioavailability[36,46]. Although the induction of vascular leakage and EC toxicity by IS and PCS were rather modest in normal 3D vessels, their deleterious impact on the endothelium might be more pronounced under disease conditions. Consistent with this, previous studies have demonstrated that the negative effects of IS on ECs can be counteracted by NO, indicating that the impact of IS depends on NO bioavailability[47]. Further studies should examine whether endothelial dysfunction preconditioned in 3D vessels could exacerbate the detrimental effects of IS or PCS. Additionally, the combination of IS and PCS or with other PBUTs might synergistically produce negative impacts on the endothelium.

Noted, the concentrations of IS and PCS used in our studies correspond to the plasma levels in CKD patients reported previously (IS = 209–1113 µM; PCS = 228–558 µM)[7,41,48]. PC is typically produced in the gut and primarily converted to PCS through sulfonation in the liver[9]; thus, PC was used in equimolar concentrations of PCS. Although to what extent PC enters the systemic circulation in CKD is still unclear, an increase in serum PC and

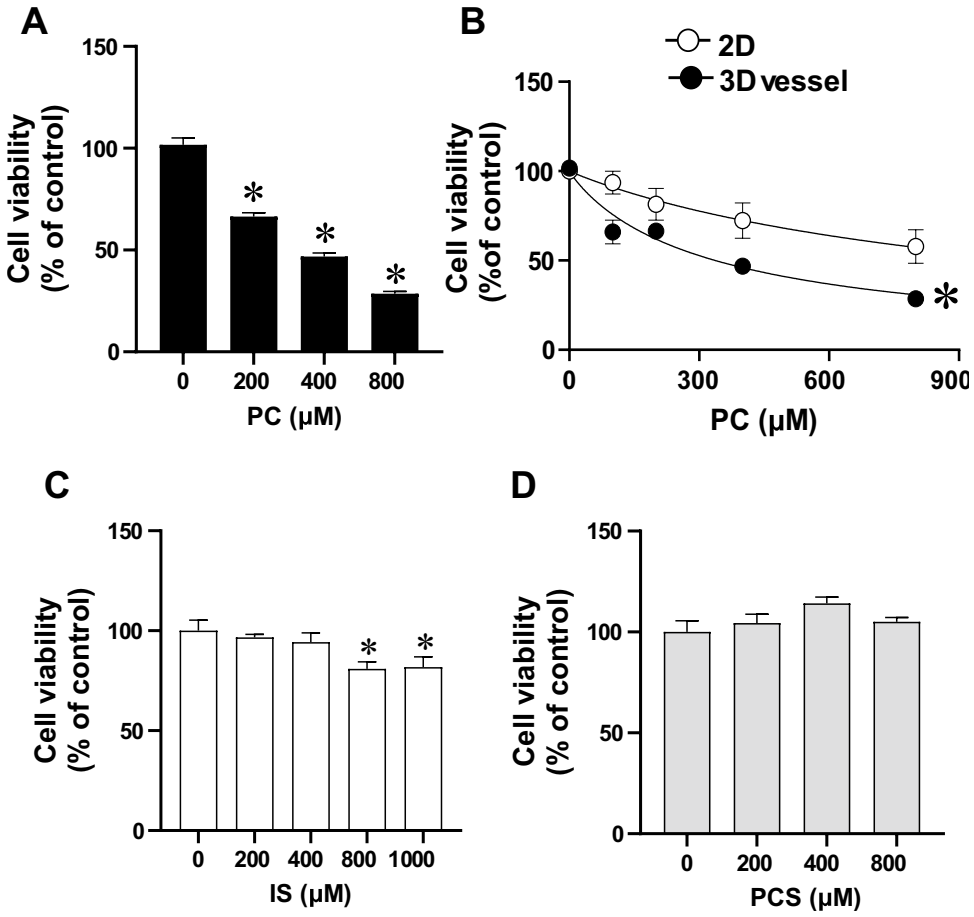

Figure 5. Endothelial toxicity to uremic toxins in treated 3D vessels. Cell viability after 72 h of stimulation with either vehicle or different concentrations of (**A**) p-cresol (PC) (n = 6–7). Data are presented as mean ± SEM, $^{*}p < 0.05$ versus control (0 μM). One-way ANOVA multiple comparisons were used. (**B**) Comparison of PC-induced cytotoxicity between 2D conventional cell cultures and 3D vessels. n = 3 for 2D and n = 7 for 3D vessels, $^{*}p < 0.05$, Two-way ANOVA, non-linear regression analysis. EC viability after 72 h of stimulation with (**C**) indoxylsulfate (IS) (n = 6) or (**D**) p-cresyl sulfate (PCS) (n = 6–8). Data are presented as mean ± SEM, $^{*}p < 0.05$ versus control (0 μM). One-way ANOVA multiple comparisons were used.

its accumulation in certain tissues such as the liver have been reported in patients undergoing hemodialysis[49,50]. PC is known to induce liver injury in vivo[51] and disrupting the gut barrier[52], indicating that more non-conjugated PC could enter circulation. Together, increased PC in patients with CKD could result in detrimental outcomes for the intestinal epithelium, liver, and blood vessels.

Although conventional 2D cultures provide a valuable tool to dissect potential mechanisms behind the role of PBUTs in causing endothelial dysfunction, they fail to recapitulate the complexity of the in vivo microenvironment[53]. Two-dimensional EC culture models may be inadequate when trying to predict the biological activities of UTs in humans. From our study, the cytotoxic effects of IS and PCS at concentrations often reported in CKD were nearly negligible in 3D vessels, which differs from 2D findings reported previously[54,55]. However, our data appear to be consistent with a previous study showing that ECs cultured in 3D ECM were resistant to uremic milieu-induced cytotoxicity compared with those in 2D cultures[56]. It has been speculated that intracellular signaling alterations in 3D cultures modify uremia sensitivity[56]. Despite the mechanisms being unclear, there might be selective changes of in EC signaling responsible for the distinct impact of different UTs in 3D vessels. This notion is supported by our observations that ECs from 3D vessels were more susceptible to PC-induced cytotoxicity compared with those from 2D culture. Possibly, specific modulators may have caused the PC effects to be more impactful in 3D vessels, however, this needs to be further investigated.

In this study, we demonstrated the utility of using OOCs to evaluate the impact of different PBUTs on the vasculature. Prolonged exposure to PC led to a significant impairment of endothelial integrity and an increase in endothelial cytotoxicity and inflammation in 3D vessels. The biological activities of different PBUTs differed, and the results from 3Dvessels did not always correlate with what was previously reported in studies using 2D cultures [57,58]. We also observed that ECs in 3D vessels are more prone to PC-induced endothelial cytotoxicity than those in 2D cultures, possibly because of changes in EC signaling that are responsible for the effects of PC when ECs were cultured in OOCs. The OOC platform employed in this study has several limitations, including bi-directional flow and the absence of precise control over shear stress. More advanced OOCs capable of

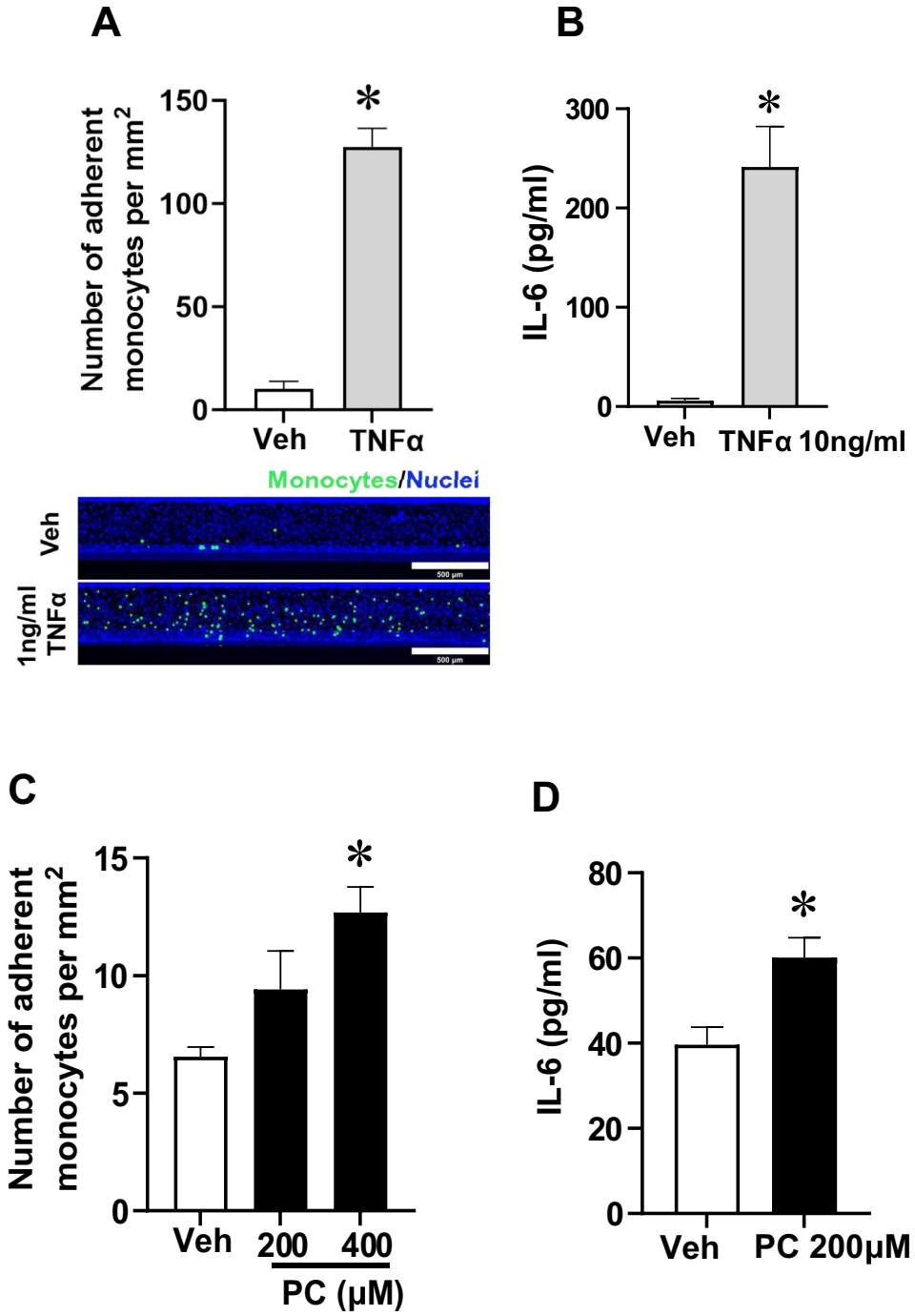

Figure 6. Inflammatory responses induced by p-cresol (PC) in 3D vessels. (**A**) Quantifications of monocyte adhesion to the endothelial surface in 3D vessels and representative images with monocytes labeled in green and nuclei staining in blue after either vehicle (Veh) or 1 ng/mL TNFα stimulation for 6 h. Magnification: 5X; scale bar: 500 µm. Data are presented as mean ± SEM, $^*p < 0.05$ versus Veh, n = 3–4, t-test. (**B**) IL-6 production in flow-through media after 3D vessels were stimulated with Veh or TNFα for 24 h. Data are presented as mean ± SEM, $^*p < 0.05$ versus Veh, n = 7, t-test. (**C**) Quantifications of monocyte adhesion to the endothelial surface in 3D vessels after either vehicle (Veh), 200, or 400 µM of PC treatment for 24 h. Data are presented as mean ± SEM, $^*p < 0.05$ versus Veh, n = 3. One-way ANOVA multiple comparisons were used. (**D**) IL-6 production from 3D vessels stimulated with PC for 24 h. Data are presented as mean ± SEM $^*p < 0.05$ versus Veh, n = 12, t-test.

providing unidirectional flow and higher magnitude of shear, both of which are important to promote endothelial function[59], will allow evaluation of UTs' impacts on the vasculature in a more physiologically relevant manner

than our current model. Nevertheless, the OOC utilized in our studies is sufficient to unmask the diverse effects of PBUTs, providing unique insights distinct from those derived from 2D cultures.

Methods

Cell cultures

Pooled primary human umbilical vein endothelial cells (HUVECs) were purchased from Promocell (C-12203, Germany). Cells were cultured in Endothelial Cell Growth Medium 2 (C-22011, Promocell) supplemented with 100 U/mL of penicillin (Gibco), 100 µg/mL of streptomycin (Gibco), and 2% fetal calf serum (FCS) (Promocell) in a humidified incubator with 5% CO_2 and 37 °C. The culture medium was renewed every two days. 3D vessels were developed using an Organoplate® 2-lane (9605–400, Mimetas, The Netherlands) that allows cells to grow in a separated channel adjacent to the extracellular matrix (ECM) (Supplementary Fig. 1A and B)[18,60]. By following the manufacturer's protocol, collagen type I (5 mg/mL, 3447–020-01, AmSbio Cultrex) was neutralized with 10% 37 g/L Na_2HCO_3 (S5761, Sigma) and 10% 1 M HEPES buffer (15630–080, Life Technologies) at 4 °C. The mixture was loaded in the ECM channels and allowed to polymerize at 37 °C overnight before cell seeding. Two microliters of HUVEC suspension (2×10^7 cells/mL) were added to the medium inlet, followed by adding culture medium to the medium inlet. The plate was placed in a humidified incubator with 5% CO_2 at 37 °C on the plate stand at 75° to allow cell adhesion to collagen. After 3 h, the culture medium was added to the medium outlet. Luminal flow was initiated by placing the plate on a rocker (OrganoFlow®, Mimetas) with an incline of 7° and an interval of 8 min (intermittent shear forces ranging between 0 and 2.2 dyne/cm^2) (Mimetas). The culture medium was refreshed every 2 days. Three-dimensional vessels were typically formed within a few days and became confluent on day 4 or 5. PC, IS, and PCS were diluted in complete medium before 3D vessel exposure at the indicated concentrations and times.

Live/dead staining

After 5 days of cell seeding, the viability of 3D vessels was assessed using a LIVE/DEAD Viability/Cytotoxicity kit for mammalian cells (L3224, ThermoFisher Scientific). Following the manufacturer's protocol, live cells were stained with green-fluorescent calcein-AM, whereas red-fluorescent ethidium homodimer-1 indicated dead cells.

Cell viability assay

The effects of PC, IS, and PCS on cell viability were tested using water-soluble tetrazolium salt (WST-8/CCK8) (ab228554, Abcam). Briefly, 3D vessels were exposed to PC, IS, or PCS for 72 h. The culture medium was removed and replaced with medium containing WST-8 solution (50 µL/chip). The cells were incubated for 30 min in a 5% CO_2 incubator at 37 °C on an OrganoFlow with an inclination of 7° and interval of 8 min. The plate was then removed from the rocker for 5 min to stop perfusion. To quantify cell viability, the orange formazan product was measured at 460 nm using a SynergyTM Neo2 Multi-Mode microplate reader (BioTek, USA). WST-8 solution without cells was used to subtract background signals. In some experiments, 100 µM cisplatin was used as a positive control for cell death, from which the reliability of the WST-8 assay was determined by a robust Z′ factor.

Permeability assay

To measure the vascular permeability of 3D vessels, we followed a previously described protocol[18]. The gel inlets were filled with 20 µL complete medium. The medium inlets and outlets of microvascular channels were infused with 0.5 mg/mL of FITC dextran 70 kDa (46945, Sigma) or 10 kDa (FD10S, Sigma). The leakage of the fluorescence dye from the luminal side of the 3D vessel to the ECM channel was monitored using Cytation™ 5 Cell Imaging Multi-Mode Reader (BioTek, USA) for time-lapse studies. Images were captured every 1 min for a total of 30 min. Permeability coefficient (Papp), a measure of the barrier integrity based on the flux of a macromolecule with a known molecular weight across a barrier[61], was calculated by quantitating fluorescence intensity in the lumen and the ECM channels of captured images using the formula below.

$$Papp = \left(\frac{dQ}{dt}\right) \times \left(\frac{Vgel}{Abarrier}\right)$$

where dQ is the intensity difference of the ECM compartment and the lumen of the 3D vessels, dt is the difference between the end and initial time points, V gel is the volume of the measured area in the ECM compartment (4.136×10^{-4} cm^3), and A barrier is the edge of the ECM compartment that interfaces with the lumen compartment (1.218×10^{-2} cm^2).

Immunohistochemistry

Cells were fixed with 4% paraformaldehyde (PFA) for 10 min at room temperature. After washing with 1X PBS, the cells were permeabilized with 0.3% Triton X-100 and blocked with blocking solution (12411S, Cell signaling) for 1 h at room temperature. Depending on experiments, 3D vessels were incubated with VE-cadherin (ab33168, Abcam) or CD31 (3528S, Cell signaling) antibody at 4 °C overnight. The cells were washed with 1 × PBS followed by incubation with either goat-anti-mouse antibody Alexa Fluor 488 (4408S, Cell Signaling) or goat-anti-rabbit antibody Alexa Fluor 555 (4413S, Cell Signaling) for 30 min. Cell nuclei were stained using Hoechst (5 µg/mL) (H3570, Invitrogen) for 15 min at room temperature. ActinRed™ 555 ReadyProbes™ Reagent (Rhodamine phalloidin) (R37112, Invitrogen) was used to stain for F-actin. In some experiments, 3D vessels were stimulated with indicated concentrations of PC or vehicle for 72 h before immunostaining. Fluorescence images were captured using maximum projection under confocal microscopy (Zeiss, Germany). Pixel to pixel to evaluate cellular co-localization of VE-cadherin and F-actin was analyzed by computing Pearson's R correlation coefficient using

Zeiss confocal microcopy software. Quantifications of the F-actin stress fibers and VE-cadherin intensity were performed using Zeiss software and normalized by the number of nuclei.

Monocyte adhesion assay

The adherence of monocytes to the endothelial surface in 3D vessels after PC treatment was evaluated following the method described previously by Poussin et al[60]. Briefly, U937 human monocytes (CRL-1593.2, ATCC) were harvested and fluorescently labeled with 10 µM Green CMFDA (AB145459, Abcam). The nuclei of ECs were counter-stained with Hoechst (H3570, Thermo Fisher Scientific). Subsequently, the labeled U937 monocytes were perfused into the medium path and allowed to adhere to endothelial surfaces for 15 min. After washing out the non-adherent monocytes, images were taken using a fluorescence microscope (Zeiss, Germany). The numbers of monocytes adhered to ECs per surface area were counted as described previously using intensity thresholding and particle detection in ImageJ[60]. In some experiments, 3D vessels were stimulated with 1 ng/mL TNFα as a positive control.

Human IL-6

Conditioned medium was collected from 3D vessels after treatment with PC for 24 h. Quantitative measurement of IL-6 production was performed using a human IL-6 ELISA kit (88–7066, Invitrogen) according to the manufacturer's instructions. Absorbance was measured using a microplate reader (BioTek Synergy Neo2, Agilent Technologies, USA).

Statistical analysis

Data are presented as mean ± standard error of the mean (SEM). Prism (v.9; GraphPad Software, San Deigo, CA, USA) was used for statistical analysis. Multiple comparison was performed either by one-way or two-way ANOVA RM with Bonferroni's post hoc test. In some experiments, the mean between two groups was compared using a t-test. All data were generated from at least two independent experiments with the number of individual 3D vessels/condition (n) indicated in each figure legend. $p \leq 0.05$ was considered significant.

To validate the cytotoxicity assays, a robust Z′ factor was calculated based on methods previously described by Bircsak et al[35]. and Zhang et al[62]. Assays with robust Z′ values greater than 0.2 were considered good for compound screening.

Data availability

All data generated or analyzed during this study are included in this published article and its supplementary information files.

Received: 2 March 2024; Accepted: 31 July 2024
Published online: 09 August 2024

References

1. McCarron, J. G., Lee, M. D. & Wilson, C. The endothelium solves problems that endothelial cells do not know exist. *Trends Pharmacol. Sci.* **38**, 322–338. https://doi.org/10.1016/j.tips.2017.01.008 (2017).
2. Yilmaz, M. I. *et al.* The determinants of endothelial dysfunction in CKD: oxidative stress and asymmetric dimethylarginine. *Am. J. Kidney Dis.* **47**, 42–50. https://doi.org/10.1053/j.ajkd.2005.09.029 (2006).
3. Roumeliotis, S., Mallamaci, F. & Zoccali, C. Endothelial dysfunction in chronic kidney disease, from biology to clinical outcomes: A 2020 update. *J. Clin. Med.* https://doi.org/10.3390/jcm9082359 (2020).
4. Jankowski, J., Floege, J., Fliser, D., Bohm, M. & Marx, N. Cardiovascular disease in chronic kidney disease: Pathophysiological insights and therapeutic options. *Circulation* **143**, 1157–1172. https://doi.org/10.1161/CIRCULATIONAHA.120.050686 (2021).
5. El Chamieh, C., Liabeuf, S. & Massy, Z. Uremic toxins and cardiovascular risk in chronic kidney disease: What have we learned recently beyond the past findings?. *Toxins (Basel)* https://doi.org/10.3390/toxins14040280 (2022).
6. Meijers, B. K. *et al.* Free p-cresol is associated with cardiovascular disease in hemodialysis patients. *Kidney Int.* **73**, 1174–1180. https://doi.org/10.1038/ki.2008.31 (2008).
7. Lin, C. J. *et al.* p-Cresylsulfate and indoxyl sulfate level at different stages of chronic kidney disease. *J. Clin. Lab. Anal.* **25**, 191–197. https://doi.org/10.1002/jcla.20456 (2011).
8. Liu, W. C., Tomino, Y. & Lu, K. C. Impacts of indoxyl sulfate and p-cresol sulfate on chronic kidney disease and mitigating effects of AST-120. *Toxins (Basel)* https://doi.org/10.3390/toxins10090367 (2018).
9. Cunha, R. S. D., Santos, A. F., Barreto, F. C. & Stinghen, A. E. M. How do uremic toxins affect the endothelium?. *Toxins (Basel)* https://doi.org/10.3390/toxins12060412 (2020).
10. Gryp, T., Vanholder, R., Vaneechoutte, M. & Glorieux, G. p-Cresyl Sulfate. *Toxins (Basel)* https://doi.org/10.3390/toxins9020052 (2017).
11. Banoglu, E., Jha, G. G. & King, R. S. Hepatic microsomal metabolism of indole to indoxyl, a precursor of indoxyl sulfate. *Eur. J. Drug. Metab. Pharmacokinet.* **26**, 235–240. https://doi.org/10.1007/BF03226377 (2001).
12. Evenepoel, P., Glorieux, G. & Meijers, B. p-cresol sulfate and indoxyl sulfate: Some clouds are gathering in the uremic toxin sky. *Kidney Int.* **92**, 1323–1324. https://doi.org/10.1016/j.kint.2017.06.029 (2017).
13. Glorieux, G. *et al.* Free p-cresyl sulfate shows the highest association with cardiovascular outcome in chronic kidney disease. *Nephrol. Dial Transpl.* **36**, 998–1005. https://doi.org/10.1093/ndt/gfab004 (2021).
14. Krukowski, H. *et al.* Gut microbiome studies in CKD: Opportunities, pitfalls and therapeutic potential. *Nat. Rev. Nephrol.* **19**, 87–101. https://doi.org/10.1038/s41581-022-00647-z (2023).
15. Schulman, G. *et al.* Randomized placebo-controlled EPPIC trials of AST-120 in CKD. *J. Am. Soc. Nephrol.* **26**, 1732–1746. https://doi.org/10.1681/ASN.2014010042 (2015).
16. Su, P. Y. *et al.* Efficacy of AST-120 for patients with chronic kidney disease: A network meta-analysis of randomized controlled trials. *Front. Pharmacol.* **12**, 676345. https://doi.org/10.3389/fphar.2021.676345 (2021).
17. Vanholder, R., Nigam, S. K., Burtey, S. & Glorieux, G. What if not all metabolites from the uremic toxin generating pathways are toxic? A hypothesis. *Toxins (Basel)* https://doi.org/10.3390/toxins14030221 (2022).

18. van Duinen, V. *et al.* 96 perfusable blood vessels to study vascular permeability in vitro. *Sci. Rep.* **7**, 18071. https://doi.org/10.1038/s41598-017-14716-y (2017).
19. Ingber, D. E. Human organs-on-chips for disease modelling, drug development and personalized medicine. *Nat. Rev. Genet.* **23**, 467–491. https://doi.org/10.1038/s41576-022-00466-9 (2022).
20. Linville, R. M. *et al.* Three-dimensional microenvironment regulates gene expression, function, and tight junction dynamics of iPSC-derived blood-brain barrier microvessels. *Fluids Barriers CNS* **19**, 87. https://doi.org/10.1186/s12987-022-00377-1 (2022).
21. Davies, P. F. Hemodynamic shear stress and the endothelium in cardiovascular pathophysiology. *Nat. Clin. Pract. Cardiovasc. Med.* **6**, 16–26. https://doi.org/10.1038/ncpcardio1397 (2009).
22. Davis, G. E. & Senger, D. R. Endothelial extracellular matrix: Biosynthesis, remodeling, and functions during vascular morphogenesis and neovessel stabilization. *Circ. Res.* **97**, 1093–1107. https://doi.org/10.1161/01.RES.0000191547.64391.e3 (2005).
23. Junaid, A. *et al.* Metabolic response of blood vessels to TNFalpha. *Elife* https://doi.org/10.7554/eLife.54754 (2020).
24. Hajal, C. *et al.* Engineered human blood-brain barrier microfluidic model for vascular permeability analyses. *Nat. Protoc.* **17**, 95–128. https://doi.org/10.1038/s41596-021-00635-w (2022).
25. Barrile, R. *et al.* Organ-on-chip recapitulates thrombosis induced by an anti-CD154 monoclonal antibody: Translational potential of advanced microengineered systems. *Clin. Pharmacol. Ther.* **104**, 1240–1248. https://doi.org/10.1002/cpt.1054 (2018).
26. Park, K. Y., Kim, S. J., Oh, E. & Heo, T. H. Induction of vascular leak syndrome by tumor necrosis factor-alpha alone. *Biomed. Pharmacother.* **70**, 213–216. https://doi.org/10.1016/j.biopha.2015.01.021 (2015).
27. Wettschureck, N., Strilic, B. & Offermanns, S. Passing the vascular barrier: Endothelial signaling processes controlling extravasation. *Physiol. Rev.* **99**, 1467–1525. https://doi.org/10.1152/physrev.00037.2018 (2019).
28. Thurston, G. & Turner, D. Thrombin-induced increase of F-actin in human umbilical vein endothelial cells. *Microvasc. Res.* **47**, 1–20. https://doi.org/10.1006/mvre.1994.1001 (1994).
29. van Geemen, D. *et al.* F-actin-anchored focal adhesions distinguish endothelial phenotypes of human arteries and veins. *Arterioscler. Thromb. Vasc. Biol.* **34**, 2059–2067. https://doi.org/10.1161/ATVBAHA.114.304180 (2014).
30. Hordijk, P. L. *et al.* Vascular-endothelial-cadherin modulates endothelial monolayer permeability. *J. Cell. Sci.* **112**(Pt 12), 1915–1923. https://doi.org/10.1242/jcs.112.12.1915 (1999).
31. Parker, W. H., Qu, Z. C. & May, J. M. Intracellular ascorbate prevents endothelial barrier permeabilization by thrombin. *J. Biol. Chem.* **290**, 21486–21497. https://doi.org/10.1074/jbc.M115.662098 (2015).
32. Junaid, A. *et al.* Ebola hemorrhagic shock syndrome-on-a-chip. *iScience* **23**, 100765. https://doi.org/10.1016/j.isci.2019.100765 (2020).
33. Dunn, K. W., Kamocka, M. M. & McDonald, J. H. A practical guide to evaluating colocalization in biological microscopy. *Am. J. Physiol. Cell. Physiol.* **300**, C723-742. https://doi.org/10.1152/ajpcell.00462.2010 (2011).
34. Kirchmair, R. *et al.* Antiangiogenesis mediates cisplatin-induced peripheral neuropathy: Attenuation or reversal by local vascular endothelial growth factor gene therapy without augmenting tumor growth. *Circulation* **111**, 2662–2670. https://doi.org/10.1161/CIRCULATIONAHA.104.470849 (2005).
35. Bircsak, K. M. *et al.* A 3D microfluidic liver model for high throughput compound toxicity screening in the OrganoPlate(R). *Toxicology* **450**, 152667. https://doi.org/10.1016/j.tox.2020.152667 (2021).
36. Dusing, P. *et al.* Vascular pathologies in chronic kidney disease: pathophysiological mechanisms and novel therapeutic approaches. *J. Mol. Med. (Berl.)* **99**, 335–348. https://doi.org/10.1007/s00109-021-02037-7 (2021).
37. Cross, J. Endothelial dysfunction in uraemia. *Blood Purif.* **20**, 459–461. https://doi.org/10.1159/000063552 (2002).
38. Alani, H., Tamimi, A. & Tamimi, N. Cardiovascular co-morbidity in chronic kidney disease: Current knowledge and future research needs. *World J. Nephrol.* **3**, 156–168. https://doi.org/10.5527/wjn.v3.i4.156 (2014).
39. Morales, J. & Handelsman, Y. Cardiovascular outcomes in patients with diabetes and kidney disease: JACC review topic of the week. *J. Am. Coll. Cardiol.* **82**, 161–170. https://doi.org/10.1016/j.jacc.2023.04.052 (2023).
40. Weiner, D. E. *et al.* The Framingham predictive instrument in chronic kidney disease. *J. Am. Coll. Cardiol.* **50**, 217–224. https://doi.org/10.1016/j.jacc.2007.03.037 (2007).
41. Vanholder, R., Schepers, E., Pletinck, A., Nagler, E. V. & Glorieux, G. The uremic toxicity of indoxyl sulfate and p-cresyl sulfate: A systematic review. *J. Am. Soc. Nephrol.* **25**, 1897–1907. https://doi.org/10.1681/ASN.2013101062 (2014).
42. Zhu, J. Z. *et al.* P-cresol, but not p-cresylsulphate, disrupts endothelial progenitor cell function in vitro. *Nephrol. Dial Transpl.* **27**, 4323–4330. https://doi.org/10.1093/ndt/gfs382 (2012).
43. Chaves, L. D. *et al.* Unconjugated p-cresol activates macrophage macropinocytosis leading to increased LDL uptake. *JCI Insight* https://doi.org/10.1172/jci.insight.144410 (2021).
44. Poesen, R. *et al.* Metabolism, protein binding, and renal clearance of microbiota-derived p-cresol in patients with CKD. *Clin. J. Am. Soc. Nephrol.* **11**, 1136–1144. https://doi.org/10.2215/CJN.00160116 (2016).
45. Cockwell, P. & Fisher, L. A. The global burden of chronic kidney disease. *Lancet* **395**, 662–664. https://doi.org/10.1016/S0140-6736(19)32977-0 (2020).
46. Drozdz, D., Drozdz, M. & Wojcik, M. Endothelial dysfunction as a factor leading to arterial hypertension. *Pediatr. Nephrol.* **38**, 2973–2985. https://doi.org/10.1007/s00467-022-05802-z (2023).
47. Kharait, S., Haddad, D. J. & Springer, M. L. Nitric oxide counters the inhibitory effects of uremic toxin indoxyl sulfate on endothelial cells by governing ERK MAP kinase and myosin light chain activation. *Biochem. Biophys. Res. Commun.* **409**, 758–763. https://doi.org/10.1016/j.bbrc.2011.05.084 (2011).
48. Duranton, F. *et al.* Normal and pathologic concentrations of uremic toxins. *J. Am. Soc. Nephrol.* **23**, 1258–1270. https://doi.org/10.1681/ASN.2011121175 (2012).
49. de Loor, H., Bammens, B., Evenepoel, P., De Preter, V. & Verbeke, K. Gas chromatographic-mass spectrometric analysis for measurement of p-cresol and its conjugated metabolites in uremic and normal serum. *Clin. Chem.* **51**, 1535–1538. https://doi.org/10.1373/clinchem.2005.050781 (2005).
50. Ikematsu, N. *et al.* Organ distribution of endogenous p-cresol in hemodialysis patients. *J. Med. Invest.* **66**, 81–85. https://doi.org/10.2152/jmi.66.81 (2019).
51. Thompson, D. C., Perera, K., Fisher, R. & Brendel, K. Cresol isomers: Comparison of toxic potency in rat liver slices. *Toxicol. Appl. Pharmacol.* **125**, 51–58. https://doi.org/10.1006/taap.1994.1048 (1994).
52. Andriamihaja, M. *et al.* The deleterious metabolic and genotoxic effects of the bacterial metabolite p-cresol on colonic epithelial cells. *Free Radic. Biol. Med.* **85**, 219–227. https://doi.org/10.1016/j.freeradbiomed.2015.04.004 (2015).
53. Giordano, L., Mihaila, S. M., Eslami Amirabadi, H. & Masereeuw, R. Microphysiological systems to recapitulate the gut-kidney axis. *Trends Biotechnol.* **39**, 811–823. https://doi.org/10.1016/j.tibtech.2020.12.001 (2021).
54. Tumur, Z. & Niwa, T. Indoxyl sulfate inhibits nitric oxide production and cell viability by inducing oxidative stress in vascular endothelial cells. *Am. J. Nephrol.* **29**, 551–557. https://doi.org/10.1159/000191468 (2009).
55. Favretto, G. *et al.* Role of organic anion transporters in the uptake of protein-bound uremic toxins by human endothelial cells and monocyte chemoattractant protein-1 expression. *J. Vasc. Res.* **54**, 170–179. https://doi.org/10.1159/000468542 (2017).
56. Chitalia, V. C. *et al.* Matrix-embedded endothelial cells are protected from the uremic milieu. *Nephrol. Dial Transpl.* **26**, 3858–3865. https://doi.org/10.1093/ndt/gfr337 (2011).
57. Dou, L. *et al.* The uremic solutes p-cresol and indoxyl sulfate inhibit endothelial proliferation and wound repair. *Kidney Int.* **65**, 442–451. https://doi.org/10.1111/j.1523-1755.2004.00399.x (2004).

58. Watanabe, H. *et al.* p-Cresyl sulfate, a uremic toxin, causes vascular endothelial and smooth muscle cell damages by inducing oxidative stress. *Pharmacol. Res. Perspect.* **3**, e00092. https://doi.org/10.1002/prp2.92 (2015).
59. Tamargo, I. A., Baek, K. I., Kim, Y., Park, C. & Jo, H. Flow-induced reprogramming of endothelial cells in atherosclerosis. *Nat. Rev. Cardiol.* **20**, 738–753. https://doi.org/10.1038/s41569-023-00883-1 (2023).
60. Poussin, C. *et al.* 3D human microvessel-on-a-chip model for studying monocyte-to-endothelium adhesion under flow - application in systems toxicology. *ALTEX* **37**, 47–63. https://doi.org/10.14573/altex.1811301 (2020).
61. Gomes, M. J., Mendes, B., Martins, S. & Sarmento, B. *Concepts and Models for Drug Permeability Studies* 169–188 (Woodhead Publishing, 2016).
62. Zhang, J. H., Chung, T. D. & Oldenburg, K. R. A simple statistical parameter for use in evaluation and validation of high throughput screening assays. *J. Biomol. Screen.* **4**, 67–73. https://doi.org/10.1177/108705719900400206 (1999).

Acknowledgements

We thank the support team from MIMETAS for technical guidance and Dr. Aungkura Supokawej, Department of Clinical Microscopy, Faculty of Medical Technology for reagents. We also thank Lisa Oberding from Edanz (www.edanz.com/ac) for editing a draft of this manuscript.

Author contributions

S.M., T.D. , T.T., and T.S. performed experiment, analyzed data, and prepared figures. C.K. conceptualized the project and provided inputs. P.K. led the project and wrote the manuscript with S.M. P.K. and K.M. discussed and revised the manuscript. P.K. and K.M. obtained the funding. All authors reviewed the manuscript.

Funding

This work was supported by Program Management Unit Competitiveness (PMU-C; C10F640323 to P.K. and K.M.) and the Faculty of Medicine of Ramathibodi Hospital Mahidol University (CF63007 to P.K.).

Competing interests

The authors declare no competing interests.

Additional information

Supplementary Information The online version contains supplementary material available at https://doi.org/10.1038/s41598-024-69124-w.

Correspondence and requests for materials should be addressed to P.K.

Reprints and permissions information is available at www.nature.com/reprints.

Publisher's note Springer Nature remains neutral with regard to jurisdictional claims in published maps and institutional affiliations.